ACS OMEGA

Open Access

http://pubs.acs.org/journal/acsodf

Article

Novel Synthesis and Biophysical Characterization of Zinc Oxide Nanoparticles Using Virgin Coconut Oil

B. Durga Lakshmi, Betha Veera Vamsi Krishna, P. Tirupathi Rao, Abhinash Marukurti, Vasudha K, Esub Basha Sk, and K Ramachandra Rao*

Cite This: *ACS Omega* 2024, 9, 38396−38408

Read Online

ACCESS | Metrics & More | Article Recommendations

ABSTRACT: One of the primary concerns in the field of green synthesis of nanoparticles (NPs) utilizing plant materials is the scarcity of high purity, challenges in achieving large-scale production, and limited global accessibility. Hygienic preparation and safe storage of plant extracts are also considerable challenges in this field. So, an investigation was started to overcome these limitations. Virgin coconut oil (VCO) in its purest form is available commercially all over the world. Also, it has high medicinal value with excellent biomedical applications. Very limited work has been reported on oils as bio reducers and stabilizers. In those reports, they used a few chemicals as mediators in the processes of synthesis and cleaning. So, to the best of our knowledge, for the first time, zinc oxide (ZnO) NPs were synthesized using VCO as a reducing and capping agent with zero chemical mediators. A comprehensive investigation of the structural, microstructural, and optical properties was reported. X-ray diffraction confirms the formation of VCO-ZnO NPs with an average crystallite size of 32.81 nm in a hexagonal structure. UV characteristics confirm quantum confinement through a well-defined SPR near 223 nm with fwhm of 67 nm and a direct band gap at 3.96 eV. FTIR reveals the capping of VCO through carboxylic functional groups, particularly the −COO− group of coconut oil at 1770 cm^{-1} with a shift of about 30 cm^{-1} compared to plain VCO. TEM confirms the polycrystalline nature with nearly spherical and 10−22 nm particle size. The zeta potential of −15.4 ± 5.0 mV signifies the stability and antiagglomeration properties. FESEM with EDS results confirms morphological excellence, the purity level of synthesized NPs (99.5%), and the prominent scalability of NPs (84.38% yield). Finally, as-synthesized VCO-ZnO NPs showed very good antioxidant (IC_{50} 78.991, 51.464, and 4.677 μg/mL in DPPH, ABTS, and FRAP assays, respectively), anti-inflammatory (IC_{50} 22.42 μg/mL in protein denaturation), antimicrobial (MIC 0.156 mg/mL for *Pseudomonas* and 0.316 mg/mL for *S. aureus*), and antidiabetic properties (IC_{50} 88.45 and 147.67 μg/mL for α-amylase and α-glucosidase assays, respectively).

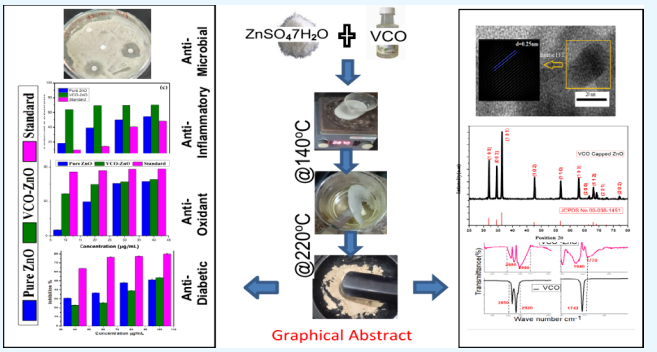

1. INTRODUCTION

The contribution of nanomaterials to society has been increasing day by day in many ways. Particularly, metal nanoparticles have enormous importance in various branches of industries and fields due to their size-dependent physical and chemical properties. The synthesis of these nanoparticles (NPs) in a physical method involves the use of costly equipment and high temperatures and pressures even though it gives stable and well-defined nanostructures. The fastest chemical approach may be suitable for nonmedical fields but not preferable for medical fields due to the chemical hazards. Also, at the end of the product's lifetime, it may lead to environmental harmfulness.

To limit the use of expensive and toxic chemicals and to reduce undesirable side effects, the best method is a green method. It has its own significance in saving energy and nature from hazardous chemicals when compared to physical and chemical methods. In this green method, which is carried out in a bottom-up approach, first, it is necessary to have an organic/inorganic precursor source. Next green reducing agents (biomolecules) are needed for the conversion of ionic precursors to atoms. This conversion is called bioreduction. Lastly, nucleation is where the atoms are joined together, forming several stable NPs with a shield of bioactivity called capping.

Over the past decade, major papers have reported plant materials as biological extracts. Most of these involve the

Received: February 22, 2024
Revised: July 20, 2024
Accepted: July 25, 2024
Published: August 30, 2024

extraction of various parts of plants. However, these plants and their extracts are globally and commercially unavailable and require energy and time in their preparation. Also, it is difficult to get organic plant materials on a large scale.[1,2] Plant products such as vegetable oils might overcome these types of limitations. Very few papers have reported the involvement of these oils in bioactive reduction. Bioactive components present in the plant extracts are mostly polyphenol compounds and flavonoids, whereas in vegetable oils bioactive components are fatty acids. Pure and unrefined virgin coconut oil (VCO) is commercially available in many countries around the world. Its fatty acid profile contains saturated (90%) and medium chain fatty acids (60%) (mainly lauric acid).[3] This abundant lauric acid next to Mother's Milk present in VCO has a few health benefits. The immediate burning capacity of triglycerides in VCO makes it not convert into cholesterol or fat. Hence, they protect against heart disease and stroke. It is a good antioxidant and is good as an anti-inflammatory, antidiabetic, etc. as per previous reports.[4,5] It is the healthiest edible oil.[6]

Among metal oxides, zinc oxide (ZnO) is quite interesting due to its high medicinal value, high thermal stability, and low cost. ZnO has been used as a mineral supplement for zinc, an essential nutrient for the human body. It is effective against diabetes mellitus as reported.[7] The acid buffering capacity of ZnO enables its use in water treatment.[8] ZnO as a direct band gap material with high exciton binding energy has excellent optical properties and applications in the semiconductor industry.[9] The high ionization energy for oxygen makes the Zn−O bond stronger. It has excellent electrical and catalytic activity, chemical stability, and environmental friendliness.[10,11] With high biocompatibility and low toxicity, ZnO has many biological applications and can be used in antimicrobial treatment, sunscreen lotions, cosmetics, etc.[12] Being a good catalytic material, ZnO has been used in many industrial products such as paints, rubber, coatings, and textiles.

Very limited research has been conducted on synthesizing NPs using oils as bioreducers and stabilizers. The reporters used acetone as a mediator in the treated oils (essential and edible oils) with precursor solutions and a few chemicals in the reduction of NPs and the cleaning process.[13−17] Zamiri reported size-controlling and antiagglomeration capacity among the ablated silver NPs in the laser ablation method.[6] However, this top-down green method has a limitation of high preparation cost in practical applications.[18] So, to the best of our knowledge in a literature review, no work has been done on the synthesis of cost-effective metal oxides using a green method without using any chemical mediators.

So this novel fabrication of VCO-capped ZnO.(VCO-ZnO) NPs with its simple method, without any chemical mediators and with high purity, would make the nanoworld healthier in the medical field. According to WHO Global Health Estimates, ischemic heart disease is terrifying the world by occupying the top spot of global causes of death. Cancer occupies the second position as the leading disease. Antioxidants play an important role in preventing these degenerative diseases.[19,20] Diabetes mellitus is also in the top 10 lists. Hence, the current study aimed to investigate the antioxidant, antidiabetic, and anti-inflammatory effects of VCO-ZnO NPs and compare them with standard medications such as ascorbic acid, metformin, and diclofenac sodium, respectively.[21] Additionally, a comparative analysis was conducted with pure ZnO to assess these biomedical activities. The pure ZnO NPs were synthesized using a conventional chemical precipitation method. Furthermore, the study explored the antimicrobial properties of these NPs, which could be beneficial in various applications, including the textile industry, water treatment, and the treatment of bacterial and fungal infection.

2. MATERIALS AND METHODS

2.1. Materials. 99.99% pure zinc sulfate heptahydrate ($ZnSO_4{\cdot}7H_2O$) was obtained from Sigma-Aldrich and virgin coconut oil from the nearby manufacturing company Konaseema Agro Products, A.P., India. Bovine serum albumin (BSA), trypsin, blood suspension, phosphate buffer, sodium acetate, tris HCl buffer, dimethyl sulfoxide (DMSO), 2,2-diphenyl-1-picrylhydraxyl (DPPH), methanol, 2,4,6-tripyridyl-*S*-triazine (TPTZ), ferric chloride ($FeCl_3$), azino-bis(3-ethyl benzothiazoline-6-sulfonic acid) (ABTS), potassium persulfate, ascorbic acid, diclofenac sodium, Luria−Bertani broth (LB Broth), triphenyl tetrazolium chloride (TTC), dinitrosalicylic acid (DNSA), and *para*-nitrophenyl-α-D-glucopyranoside (PNDGP) were obtained from Himedia Laboratories. *Staphylococcus aureus* (*S. aureus*) and *Pseudomonas* bacterial and *Candida* fungal cultures were obtained from MTTC, Chandigarh, India.

2.2. Characterization. For confirming quantum confinement of VCO-ZnO NPs, UV−vis optical absorption spectra in the wavelength range of 200−800 nm were obtained using a Shimadzu UV-2600 instrument. For functional group analysis and hence the confirmation of VCO functional groups present in VCO-ZnO NPs, Fourier transform infrared spectra were obtained at room temperature using the FTIR instrument Bruker Alpha-II with a liquid-nitrogen-cooled HgCdTe detector at 4 cm^{-1}, and the spectra were averaged over 500 scans in the mid-IR range (400−4000 cm^{-1}). Both instruments are available at the Central Instrumentation Lab, GC(A), Rajahmundry, AP, India. To determine the phase purity and morphology of the VCO-ZnO NPs, XRD and TEM characterizations were performed at Sprint Testing Solutions, Mumbai, India. To study the size distribution and zeta potential, a DLS study report of the synthesized NPs was obtained from MNIT, Jaipur, India. To get the surface morphology, purity, and percent yield, FESEM with EDS characterizations were done at GITAM, AP, India.

2.3. Methods. *2.3.1. Synthesis of VCO-ZnO NPs.* 10 g of $ZnSO_4{\cdot}7H_2O$ precursor was added to 100 mL of VCO directly and stirred thoroughly for 1 h at room temperature. With its rich amounts of saturated fats, unrefined VCO has a high boiling point of ∼220 °C and has a smoking point of 1700 °C. So the solution mixture was heated below the smoking point at ∼140 °C for 4 h in a hot air oven and allowed to cool to room temperature. A gel-like formation was obtained at the bottom of the solution. The gel was collected using filter paper and dried at 220 °C for 15 min or until the oil completely evaporated. This approach of synthesis is called the gel combustion route method.[22] Finally, the sample was calcinated to 300 °C for 3 h, ground into a fine powder, and stored safely for further use.

2.3.2. In Vitro Antioxidant Activity. The synthesized pure ZnO and VCO-ZnO NPs (samples) were adequately assessed for *in vitro* antioxidant activity by three different methods, namely a free radical scavenging DPPH assay, a ferric reducing antioxidant power (FRAP) assay, and a cationic radical scavenging ABTS assay.[23,24] All these activities were carried out in gradient concentrations of samples from 10 to 40 μg/mL.

https://doi.org/10.1021/acsomega.4c01727
ACS Omega 2024, 9, 38396−38408

In the DPPH method, methanol solutions of samples at selected concentrations were added to a 3×10^{-2} mM methanol solution of DPPH. DPPH with methanol was used as a control. In the FRAP method, the FRAP reagent was prepared using 0.01 M TPTZ in 0.04 M HCl, 0.02 M $FeCl_3$ and 0.3 M acetate buffer (pH 3.5) in 1:1:10 (v/v/v) proportion. Then, selected concentrations of acetate solutions of samples in acetate buffer were added to the prepared FRAP reagent. In this assay the control was FRAP with acetate buffer. In the ABTS method, the first ABTS reagent was prepared using 7 mM ABTS and 2.45 mM potassium persulfate in a 1:1 ratio. The reagent was preincubated overnight in the dark and diluted in methanol. Then the selected concentrations of aqueous solutions of samples after 15 min of sonication were added to that reagent. Distilled water with ABTS reagent was used as a control.

All three method reaction mixtures including ascorbic acid as a standard were subjected to 30 min of incubation in the dark at ambient temperature and centrifuged at 5000 rpm for 5 min. UV absorbances of the mixture as well as of the control at 517, 593, and 734 nm for DPPH, FRAP, and ABTS assays, respectively, were noted. The inhibition percentage was calculated using a standard formula.[25] Further interpretation of results was done by determining an important biological parameter known as efficient concentration 50 (EC_{50}) or inhibitory concentration 50 (IC_{50}) using a standard function four-parameter (A, B, C, D) logistic function (sigmoidal) in an online IC_{50} calculator.[26] The higher the antioxidant activity, the lower the value of IC_{50}.[25]

2.3.3. In Vitro Anti-inflammatory Activity. The anti-inflammatory activity of as-synthesized samples was also tested by three different *in vitro* methods, namely protein denaturation, proteinase denaturation, and heat-induced RBC hemolysis assays,.[27] All these activities were carried out in gradient concentrations of samples from 10 to 40 μg/mL. Diclofenac sodium was used as a standard, and phosphate buffer solution was used as the control for all three experiments.

In the proteinase denaturation inhibition assay, the reagents 0.05 mg of trypsin and Tris HCl (pH 7.4) were added with selected concentrations of samples and standard along with control and incubated at 37 °C for 5 min. Then, 48 μg of casein hydrolysate was added to all the mixtures and again kept at 20 min incubation at the same temperature. Finally, after incubation, the mixtures were added to 70% perchloric acid and allowed to cool at room temperature. Later, they were centrifuged at 3000 rpm for 5 min.

In the protein denaturation inhibition assay, the reaction mixtures (phosphate buffer saline (pH 6.4), 1% BSA, and various concentrations of test samples) were subjected to 15 min of incubation at 37 °C and then 5 min of heat (70 °C) was further supplied. The solutions were cooled to room temperature. Then, they were centrifuged at 3000 rpm for 5 min.

In heat-induced hemolysis, heparinized chicken blood was centrifuged at 5000 rpm for 5 min; the supernatant was removed and washed thrice with an equal volume of physiological saline (0.9% NaCl). The obtained blood volume was resuspended in 10% PBS (7.4) (v/v). Then, the reaction mixtures (blood suspension, PBS 7.4, and various concentrations of sample NPs) were incubated at 54 °C for 20 min in a shaking water bath and centrifuged at 2500 rpm for 5 min. The supernatant mixtures' UV absorbances at 210, 660, and 540 nm for protein denaturation, proteinase denaturation, and heat-induced RBC hemolysis assays, respectively, were noted. The percent inhibition in three assays was calculated by the standard formula. The Inhibitory concentration 50 (IC_{50}) values were also determined as per the reference given in the previous section.

2.3.4. Antimicrobial Activity. The evaluation of antimicrobial activity was performed by an agar-based Kirby−Bauer disc diffusion method.[28] The method is simpler and faster than the broth-based method.[29] The prepared potato dextrose agar (PDA) medium an nutrient agar medium underwent sterilization at 121 °C and 15 lb pressure for 20 min by using an autoclave. The molten medium was placed in sterile Petri dishes and allowed to cool. The selected bacterial and fungal cultures were spread on the prepared solid medium. To test the significant antimicrobial activity of synthesized NPs against the selected Gram-positive (*S. aureus*) and Gram-negative (*Pseudomonas*) pathogenic bacteria and fungal culture (*Candida*), various concentrations were chosen based on minimum inhibitory concentration values. Sterilized Whatman filter paper discs of around 6 to 8 mm size were coated with sample solutions (sonicated for better mixing of sample in water) and placed on the culture. Bacterial culture plates were incubated at 37 °C for 24 h, and the fungal culture was incubated at 24 °C for 48 h.

2.3.5. In Vitro Antidiabetic Activity. To determine the activity against one of the growing challenging diseases, diabetes, the synthesized VCO-ZnO NP samples were tested at selected concentrations (20−100 μg/mL) in both α-amylase and α -glucosidase inhibition assays as per previous works.[30,31] First, 0.02 and 0.1 M sodium phosphate buffers (SPBs) were prepared and their pH was adjusted to 6.9 by adding 6 mM NaCl. For the α-amylase (α-glucosidase) inhibition assay, 1 mL of sample was mixed in respective mounts of 0.02 M (0.1 M for α-glucosidase) SPB and 250 μL (150 μL for α-glucosidase) of 1U alpha-amylase (0.1 U α-glucosidase). The mixture was incubated for 20 min at 37 °C. After that 250 μL (50 μL for α-glucosidase) of 1% starch solution (2 mM *para*-nitrophenyl for α-glucosidase) in 0.02 M (0.1 M for α-glucosidase) SPB was added to the above mixture and again incubated for 15 min at 37 °C. The reaction was terminated by adding 1 mL of DNSA (50 μL of 0.1 M sodium carbonate for α-glucosidase). The α-amylase mixture was incubated for 10 min in a water bath at 100 °C. The same was done for selected concentrations, and the absorbance at 540 nm (405 nm) was noted. Metformin was used as a standard for a comparative study. The inhibition percentage of both assays was calculated using the standard formula.

3. RESULTS AND DISCUSSION

3.1. UV−Vis Data Interpretation. Novel optical characteristics emerge when the size of particles becomes smaller than 100 nm. UV−visible absorption spectroscopy is a well-known, fast technique to study the optical properties of newly synthesized nanomaterials. In the present paper, quantum confinement, type, and value of band gap of as prepared VCO-ZnO NPs were reported as the UV−vis absorption data.

As the minimum UV region of transparency for water is 190 nm, a sonicated aqueous solution of VCO-ZnO NPs with a concentration of 0.1 mM was taken for the UV−vis absorption spectrum and was obtained as shown in (Figure 1). It shows a surface plasmon resonance (SPR) band at 220−260 nm with a peak position at about 223 nm. This intense well-defined SPR

https://doi.org/10.1021/acsomega.4c01727
ACS Omega 2024, 9, 38396−38408

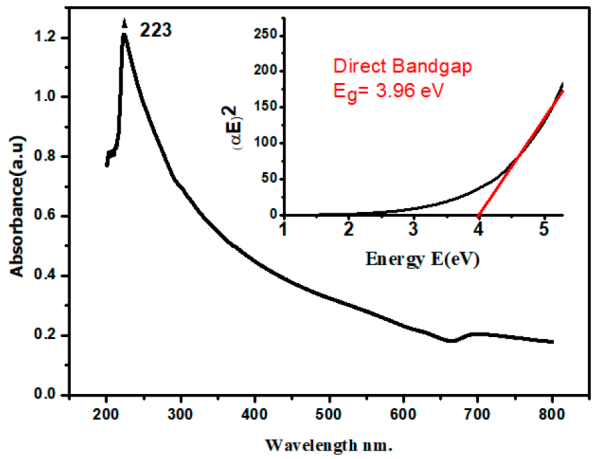

Figure 1. UV−vis spectrum of biosynthesized ZnO NPs using virgin coconut oil.

near 223 nm with a full width at half-maximum (fwhm) of about 80 nm shows the use of VCO in reducing the particle size distribution. An fwhm of less than 100 nm is normally considered as the signature of narrow particle distribution.[13]

This excitonic absorption peak at about 223 nm for VCO-ZnO NPs lies much below the excitonic absorption peak at 373 nm for bulk ZnO.[32] This blue shift in the absorption clearly indicates the quantum confinement of the VCO-ZnO NPs. In the quantum confinement range, as the particle size decreases, discrete energy levels play a role rather than continuous bands. Hence then the band gap of the particles increases. The value of this band gap energy can be accurately determined to explain the photophysical and chemical properties of semiconducting materials. As the prepared semiconducting material shows a negligible absorbance at lower energies, the Tauc plot method may be used to determine the band gap using the formula[33]

$$(\alpha E)^{\gamma} = A(E - E_g)$$

where α is the absorption coefficient, E is the photon energy, A is a constant relative to the material, and γ is either 2 for a direct transition or 1/2 for an indirect transition. Hence, the optical band gap for the absorption peak can be obtained by linear region extrapolation as shown in the inset of Figure 1. The band gap of VCO-ZnO is obtained at ∼3.96 eV. The shift is about 0.59 eV compared with bulk ZnO (E_g = 3.37 eV).[34] No linear relation was found for n = 1/2, suggesting that as-synthesized VCO-ZnO nanostructures have a direct transition. The absence of the characteristic absorption of lauric acid (n→ π^* ≈ 280−290 nm) might also indicate the coordination complex formation of ligands.

3.2. XRD Analysis. The XRD pattern of VCO-ZnO NPs is shown in Figure 2. The well-defined, narrow, high-intensity peaks reveal the nanocrystalline phase formation. The reflected intensities against detector angle 2θ are observed at 31.9, 34.58, 36.38, 47.70, 56.75, and 63.01°, which are indexed as (100), (002), (101), (102), (110), (103), (200), (112), (201), and (202), respectively, in agreement with the Joint Committee on Powder Diffraction Standards (JCPDS) card number 00-036-1451. The calculated cell parameters (using the method of TJB Holland & SAT Redfern 1995 "Unit Cell" software) are 3.2496 and 5.2065 Å, which also coincide well with JCPDS data (Table 1). The percentage of contraction of calculated d-spacing using Bragg's law from JCPDS d-spacing

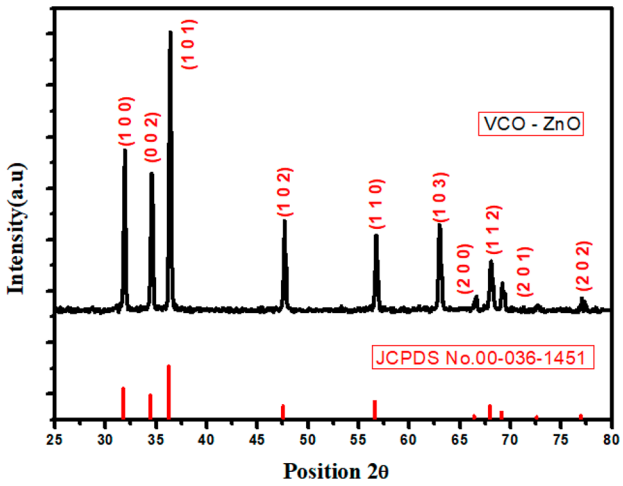

Figure 2. X-ray diffraction pattern of VCO-ZnO NPs and JCPDS reference pattern.

Table 1. Unit Cell Parameters of VCO-ZnO NPs

parameter	VCO-ZnO	JCPDS data
$a = b$ (Å)	3.2496	3.2498
c (Å)	5.2065	5.2066
volume (10^6 pm^3)	47.61	47.62

data was less than 0.5% (Table 2). This qualitative comparison with the standard crystallographic database confirms the formation of ZnO in a hexagonal crystal system with a wurtzite structure and $P6_3mc$ space group.[35] Phase purity was confirmed through the absence of additional peaks within the resolution limit of the diffractometer. Broadening of the XRD peak can be calculated by its full width at half-maximum (fwhm), a suitable XRD parameter for the determination of the average crystalline size. Using a nonlinear Gaussian curve fit, the average fwhm was obtained at 0.4°. Using the Debye−Scherrer formula (D = 0.9 λ/β cos θ, where θ is the diffraction angle, λ = 1.5406 Å, and β is fwhm), the VCO-ZnO crystallite size was determined to be around 32.8 nm.[35]

Table 2. Percent Contraction of d-Spacing Values from Calculated and JCPDS Data

2θ (deg)	d-spacing (Å)	JCPDS data (Å)	contraction (%)
31.90	2.8034	2.8143	0.38
34.58	2.5914	2.6033	0.45
36.38	2.4674	2.4759	0.34
47.70	1.9048	1.9111	0.32
56.75	1.6209	1.6247	0.23
63.01	1.4739	1.4771	0.21

3.3. FTIR Data Interpretation. The mechanism of bio reduction of NPs in green synthesis is still incompletely determined. So, the present FTIR study tries to identify the contribution of functional groups present in VCO in the formation of ZnO NPs as well as the prevention of NP agglomeration. This qualitative chemical analysis reveals the presence of stretching and bending vibrations of Zn−O, C−O, $-CH_3$, $-CH_2$, C═O, and O−H(C−H) functional groups with absorption peaks at 520, 1130, 1480, 1640, 1770, and broad 2828−2980 cm^{-1}, respectively. When compared with the FTIR spectrum of plain VCO, the sample spectrum almost

https://doi.org/10.1021/acsomega.4c01727
ACS Omega 2024, 9, 38396−38408

matches it (Figure 3). A small shift in vibrational frequency and a change in intensity (Table 3) can be interpreted by the interrelation of ZnO NPs with the functional groups in VCO.

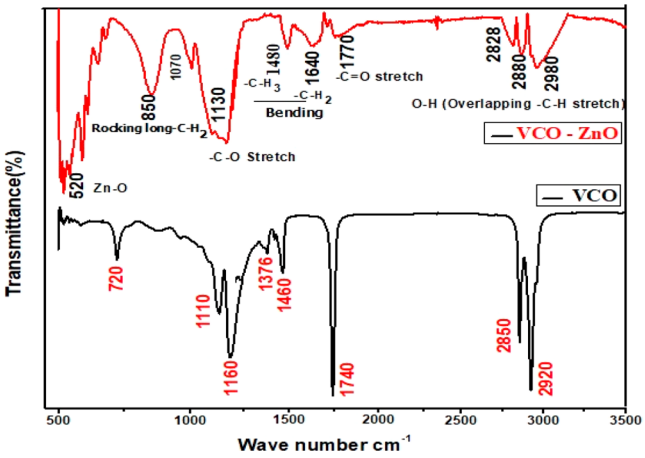

Figure 3. Fourier transform infrared spectra of VCO-ZnO and VCO.

Table 3. Functional Groups Corresponding to FTIR Peak Positions of VCO-ZnO and VCO

VCO (cm^{-1})	VCO-ZNO (cm^{-1})	shift	functional group/bond
	520, very intense		stretching vibrations of Zn−O bonds
720	850	130	rocking motion of long chain $-CH_2$ group
1160	1130, high intensity	30	stretching vibrations of −C−O
1376, 1460	1480, 1640, low intensity	104	bending vibrations of $-C-H_3$ and $-C-H_2$
1740	1770, low intensity	30	stretching vibrations of −C═O
2850, 2920	2828, 2880, 2980, medium intensity and broad	20−60	stretching vibration of −O−H in acids (usually overlaps −C−H stretching of $-C-H_3$ and $-C-H_2$)

A very broad O−H stretch band is seen along with the C═O peak, almost certainly indicating carboxylic acid. As reported earlier, the medium-chain triacyl glycerides (TAGs) account for approximately half of all types of TAGs in coconut oil.[36] There is a possibility of capping of TAG. However, TAG might decompose into medium chain fatty acids (MCFAs) and glycerol groups during the process.

The rich contributor to MCFAs is lauric acid ($CH_3-(CH_2)_{10}-C-OH$), which makes up half of the fatty acids in coconut oil. So, it signifies the possibility of bonding of polar carboxylic groups (mostly lauric acid) with ZnO NPs and hence might be involved in the bioreduction of NPs. These metal carboxylates Zn(COO−) were confirmed through broad, intense absorption peaks at a vibrational frequency of 1130 cm^{-1}.[13] Lighter H^- ions from −COO−H groups areexpected to share partially with heavy ZnO and hence form capped ZnO NPs (Figure 4).[13] The broad absorption band at 2828−2980 cm^{-1} signifies the symmetric and asymmetric stretching of methyl and methylene groups. The rocking motion of four or more $-CH_2$ groups is associated with the band at 865 cm^{-1} and is called a long chain band. This long nonpolar carbon chain could prevent the agglomeration of NPs through steric repulsion.

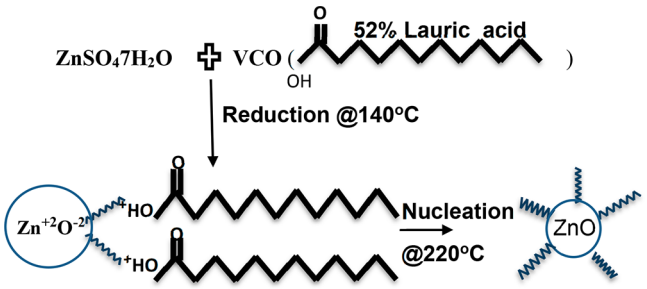

Figure 4. Possible reaction mechanism of the formation of VCO-ZnO NPs.

3.4. TEM and Selected Area Diffraction Analysis. To understand the morphology of VCO-ZnO NPs, a nanosize characterization tool, a transmission electron microscope (TEM), was used to get the lattice fringe width and particle size. Figure 5a,b clearly shows the formation of NPs with sizes ranging from 10 to 22 nm and with spherical and rod-like structures. ImageJ software was used to find the mean particle size and was obtained as 16 nm. These TEM images also depict the capping of VCO on ZnO, which prevents agglomeration of NPs. The particle size distribution is shown in Figure 5c. Using inverse FFT analysis as shown in Figure 5d, the calculated lattice fringe spacing is ∼0.25 nm, which coincides well with the *d*-spacing value from XRD. The crystallinity of synthesized VCO-ZnO NPs is also confirmed by the SAED pattern as given in Figure 5e. The ring pattern shows the polycrystallinity of the sample material and was indexed by calculating *d*-spacing values using ImageJ software and by matching with JCPDS card no. 361451 as shown in Table 4

3.5. *In Vitro* Antioxidant Activity. To measure the presence and activity of antioxidants in synthesized VCO-ZnO NPs, an *in vitro* study was done with three types of electron-transfer-based assays, namely DPPH, FRAP, and ABTS.[37] Each method has pros and cons.[38] To avoid the problem of underestimation and overestimation of total antioxidant capacity, these three standard methods were chosen.[39,40] The quantitative details of percent inhibition of DPPH by VCO-ZnO NPs are given in Table 5. Here, we calculated IC_{50} values directly by taking the mean of percent activity at gradient concentrations of samples using the online calculator mentioned in section 2.3.2. The visual representations of percent of inhibitory activity and IC_{50} values of the samples along with ascorbic acid as standard for each assay are depicted in Figure 6 and Table 6, respectively. The correlation of IC_{50} values of VCO among the three assays is matched with that of VCO-ZnO.[24] All assays were done in triplicate, and the results were obtained with very minimal standard errors (∼0.001 to 0.5).

In the DPPH assay, the absorption of DPPH at 517 nm decreased slowly with the increase of concentration of synthesized samples in a solution containing DPPH. It is shown in Figure 6 in terms of visual representation of the mean and standard deviations of percent of inhibition. Nearly comparable percents of free radical scavenging activity were observed for pure ZnO (21.0%) and VCO-ZnO (30.3%) at 40 μg/mL but were not comparable with that of the standard (92.8%). In the ABTS assay, a higher percentage of inhibitory activity was shown by pure ZnO (64.4%) than by VCO-ZnO (38.9%) at 40 μg/mL. Whereas in the FRAP method, VCO-

https://doi.org/10.1021/acsomega.4c01727
ACS Omega 2024, 9, 38396−38408

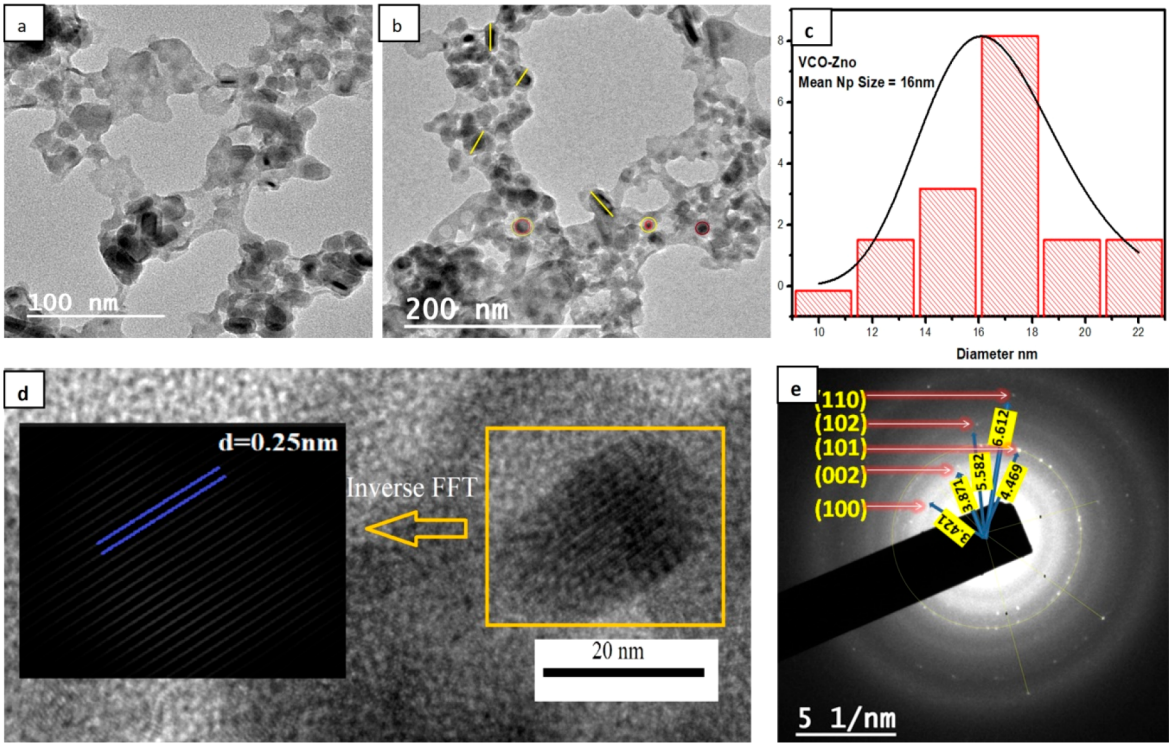

Figure 5. Transmission electron micrographs of VCO-ZnO NPs: (a) image at 100 nm scale; (b) image at 200 nm scale. (c) Size distribution histogram. (d) Inverse FFT. (e) SAED pattern.

Table 4. Calculated *d*-Spacing Values and *hkl* Indexing of SAED Ring Pattern

	d-spacing (Å)	JCPDS data (Å)	*hkl*
R_1	2.9231	2.8143	100
R_2	2.5833	2.6033	002
R_3	2.2376	2.4759	101
R_4	1.7915	1.9111	102
R_5	1.5124	1.6247	110

ZnO showed a higher radical inhibition capacity of 82% at 40 μg/mL which is nearly comparable with the percemt inhibition of ascorbic acid. The calculated IC_{50} values of VCO-ZnO were obtained at 78.991 and 51.464 μg/mL in both DPPH and ABTS assays, respectively, whereas in the FRAP assay, the IC_{50} value of VCO-ZnO was obtained at a much lower value, 4.6 μg/mL, which proved that VCO-ZnO is a good antioxidant.

3.6. *In Vitro* Anti-inflammatory Activity. The *in vitro* inhibition activity in protein/albumin denaturation, proteinase denaturation, and heat-reduced RBC hemolysis assays were used to measure the anti-inflammatory properties of pure ZnO and VCO-ZnO which are compared to the standard diclofenac sodium. The quantitative details of percent inhibition activity of VCO-ZnO for Protein denaturation are given in Table 7.

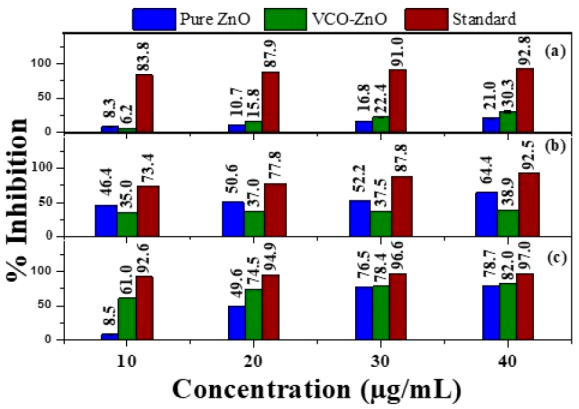

Figure 6. Percentage inhibition of (a) DPPH, (b) ABTS, and (c) FRAP at different concentrations of pure ZnO, VCO-ZnO, and ascorbic acid.

Here also, we calculated IC_{50} values directly by taking the mean of percent activity at gradient concentrations of samples using an online calculator.[26] The visual representation of the mean and standard deviations of percent of inhibition and IC_{50} values are represented in Figure 7 and Table 8, respectively. All

Table 5. Triplicate Results of Antioxidant Activity for VCO-ZnO in DPPH Method and IC_{50}

	inhibition (%)				
concentration (μg/mL)	trial 1	trial 2	trial 3	mean ± SD	IC_{50} (μg/mL)
10	06.372	5.882	6.209	6.154 ± 0.144	**78.991**
20	15.359	16.503	15.523	15.795 ± 0.357	
30	23.039	22.059	22.059	22.386 ± 0.327	
40	31.007	30.372	29.471	30.283 ± 0.446	

https://doi.org/10.1021/acsomega.4c01727
ACS Omega 2024, 9, 38396−38408

Table 6. IC_{50} Measures against Various Biological Components of *In Vitro* Antioxidant Activity

sample	IC_{50} (μg/mL)		
	DPPH	ABTS	FRAP
pure ZnO	28.632	79.440	19.054
VCO-ZnO	**78.991**	51.464	04.677
ascorbic acid	22.945	25.835	19.492
VCO[24]	93.918	43.599	10.780

assays were done in triplicate and the results obtained with very minimal standard errors (~0.000 to 0.300).

In a comparison of anti-inflammatory activity of VCO-ZnO with that of pure ZnO, the highest percent of inhibitory activity was shown by pure ZnO for protein denaturation (75.11%) and heat-induced RBC hemolysis assays (11.80%), whereas for the proteinase denaturation assay the highest percent of inhibitory activity (70.35%) was shown by VCO-ZnO at 40 μg/mL. In the protein denaturation assay the IC_{50} values for pure ZnO and VCO-ZnO are found to be 20.21 and 22.42 μg/mL, respectively. VCO-ZnO showed lower IC_{50} values for both proteinase denaturation and heat-induced RBC hemolysis, which are 4.46 and 5.099 μg/mL, respectively, than for pure ZnO. Contradictory results for percent of inhibition and IC_{50} values were found in heat-induced RBC hemolysis. With these lower IC_{50} values in all three assays, it is observed that synthesized VCO-ZnO NPs show strong anti-inflammatory properties.

3.7. Antimicrobial Activity. The antimicrobial activity of pure ZnO and VCO-ZnO NPs with different concentrations was applied against clinically significant pathogenic microorganisms, and their sensitivity in terms of zone of inhibition (ZOI) was tested in triplicate. From Figure 8, the ZOI that appeared around the disc coated with VCO-ZnO NPs clearly showed a significantly higher growth of inhibition against pure ZnO for *Pseudomonas* and *Candida*. However, a growth comparable with that if pure ZnO was found for *S. aureus* bacteria at 0.5 mg/mL. Increased antimicrobial activity was observed proportionally with the higher concentration. The bar graph representation of the mean and standard deviation of ZOI is shown in Figure 9. The synthesized VCO-ZnO NPs were equally active in the inhibition of the selected pathogens *Pseudomonas* (21.6 mm), *S. aureus* (25.00 mm), and *Candida* (17.9 mm) at 1 mg/mL concentration. These outcomes concurred with those of ZnO NPs from previous reports.[41,42] The observed white annulus might indicate the spread of fatty acid functional groups present in synthesized VCO-ZnO NPs.

3.8. *In Vitro* Antidiabetic Activity. α-Amylase and α-glucosidase enzyme inhibition is necessary to control blood glucose levels in diabetic patients. The inhibitory activity of VCO-ZnO NPs was assessed by calculating the percentage of inhibition in both assays conducted in triplicate. The quantitative information detailing the percentage of inhibition

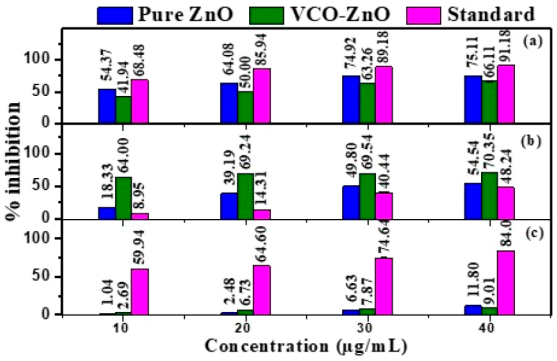

Figure 7. Percentage inhibition of (a) protein denaturation, (b) proteinase denaturation, and (c) heat-induced hemolysis at different concentrations of pure ZnO, VCO-ZnO, and diclofenac sodium.

Table 8. IC_{50} Measures against Various Biological Components of *In Vitro* Anti-inflammatory Activity

sample	IC_{50} (μg/mL)		
	protein denaturation	proteinase denaturation	heat-induced RBC hemolysis
pure ZnO	20.218	16.477	38.109
VCO-ZnO	**22.423**	04.467	5.099
diclofenac sodium	04.696	25.508	33.393

activity of VCO-ZnO for α-amylase assays can be found in Table 9. The visual representation of the mean and standard deviations of percent of inhibition is shown in Figure 10. The percentage inhibition increased with increased concentration of VCO-ZnO NPs, ranging from 20.26% (20 μg/mL) to 62.82% (100 μg/mL) for α-amylase and from 19.75% (20 μg/mL) to 53.43% (100 μg/mL) for α-glucosidase. The inhibitory potential of VCO-ZnO NPs on α-amylase is nearly equivalent to that of metformin at a concentration of 100 μg/mL. However, for α-glucosidase, a concentration of more than 100 μg/mL was needed. At the highest selected concentration, VCO-ZnO showed more antidiabetic activity than pure ZnO. The calculated IC_{50} values by taking the mean of percent activity at gradient concentrations of samples using an online calculator[26] are given in Table 10, indicating that VCO-ZnO showed better α-amylase enzyme inhibition than α-glucosidase enzyme inhibition.

3.9. Stability, Purity, and Scalability of synthesized VCO-ZnO NPs. *3.9.1. Stability of VCO-ZnO NPs: DLS Analysis.* The DLS study (Malvern Instruments Ltd.) is utilized to investigate the size distribution, polydispersity index (PDI), and zeta potential of VCO-ZnO NPs in the colloidal solution quantitatively. The average size distribution is obtained as ~200 ± 60 nm (Figure 11a). This larger size distribution is attributed to the DLS, providing a hydrodynamic diameter of NPs in the hydrated state or capping of

Table 7. Triplicate Results of Anti-inflammatory Activity in Protein Denaturation Method for VCO-ZnO NPs and and IC_{50}

concentration (μg/mL)	inhibition (%)				IC_{50} (μg/mL)
	trial 1	trial 2	trial 3	mean ± SD	
10	41.935	41.935	41.935	41.935 ± 0.000	**22.423**
20	50.000	50.000	50.000	50.000 ± 0.000	
30	63.014	63.014	63.758	63.262 ± 0.248	
40	66.038	66.460	65.823	66.107 ± 0.187	

https://doi.org/10.1021/acsomega.4c01727
ACS Omega 2024, 9, 38396−38408

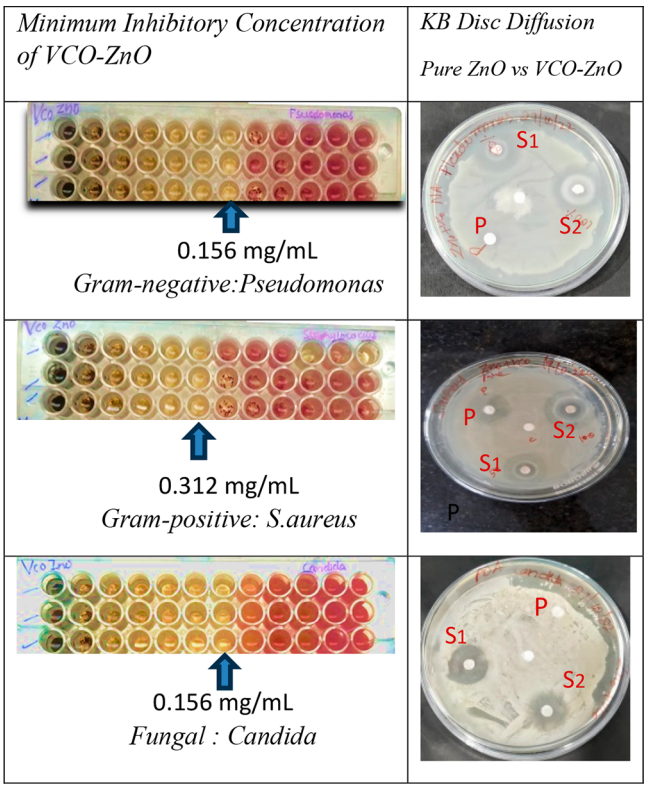

Figure 8. MIC results and visual representation of zone of inhibition of pure ZnO at 0.5 mg/mL (P) and VCO-ZnO at 0.5 mg/mL (S_1) and 1 mg/mL (S_2) concentrations against selected pathogens.

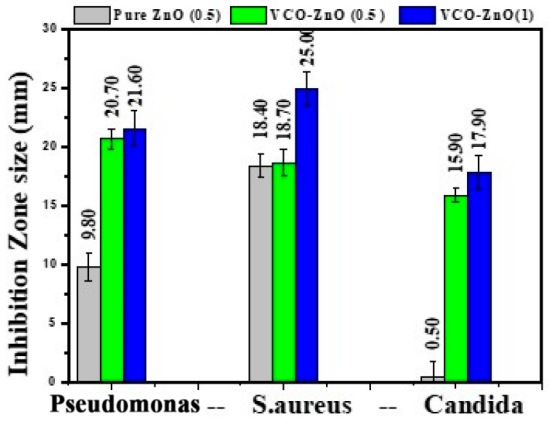

Figure 9. Zone of inhibition of pure ZnO and VCO-ZnO NP activity at different concentrations against the bacteria *Pseudomonas* and *S. aureus* and fungus *Candida*.

VCO over the surface of ZnO NPs. The lower PDI (0.141) indicates the monodisperse nature of VCO-ZnO NPs and also

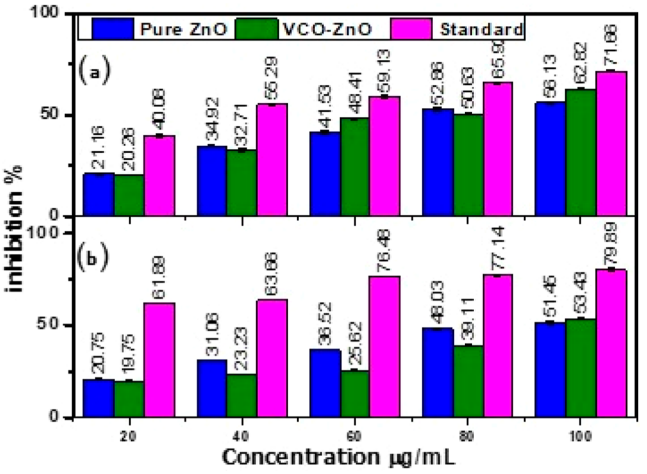

Figure 10. Percentage inhibition in (a) α-amylase and (b) α-glucosidase assays at different concentrations of pure ZnO, VCO-ZnO, and metformin.

Table 10. IC_{50} Measures against α-Amylase and α-Glucosidase of *In Vitro* Antidiabetic Activity

	IC_{50} (μg/mL)	
sample	α-amylase	α-glucosidase
pure ZnO	46.35	99.56
VCO-ZnO	**88.45**	147.67
metformin	49.56	114.19

implies control over the synthesis process, resulting in VCO-ZnO NPs with uniform sizes.[43] The zeta potential is a measurement of the electric charge that is on the surface of particles and is used to determine the colloidal stability. The zeta potential of VCO-ZnO NPs in distilled water is -15.4 ± 5 mV as shown in Figure 11b, indicating its high stability and prevention of agglomeration due to the strong electrostatic repulsive forces between NPs.

3.9.2. Purity and Scalability. One of the best techniques to determine the purity of a sample is energy dispersive spectroscopy (EDS). The quantity analysis and EDS labeled peaks show an almost 99.5% purity of the sample. Using this percentage of purity, the precursor ($ZnSO_4 \cdot 7H_2O$) weight (10 g) and its molecular weight (287.56 U), VCO-ZnO NP weight after drying (2.4 g) and molar mass of ZnO (81.38 U), we calculated the percent yield of NPs in the online Nanoparticle Yield Calculator InstaNANO (https://instanano.com/all/characterization/other/yield/ (accessed April 7, 2024)). The results are presented in Table 11. The quantification study shows a yield of 84.38% of ZnO NPs, indicating the potential for commercial production of ZnO NPs on a larger scale without causing harm to the environment through the disposal

Table 9. Triplicate Results of Antidiabetic Activity in α-Amylase Assay for VCO-ZnO and IC_{50}

	inhibition (%)				
concentration (μg/mL)	trial 1	trial 2	trial 3	mean ± SD	IC_{50} (μg/mL)
20	20.196	19.816	20.756	20.256 ± 0.273	**88.452**
40	33.273	31.813	33.053	32.713 ± 0.454	
60	47.706	48.706	48.806	48.406 ± 0.351	
80	50.726	51.226	49.926	50.626 ± 0.378	
100	63.522	62.322	62.622	62.822 ± 0.360	

https://doi.org/10.1021/acsomega.4c01727
ACS Omega 2024, 9, 38396−38408

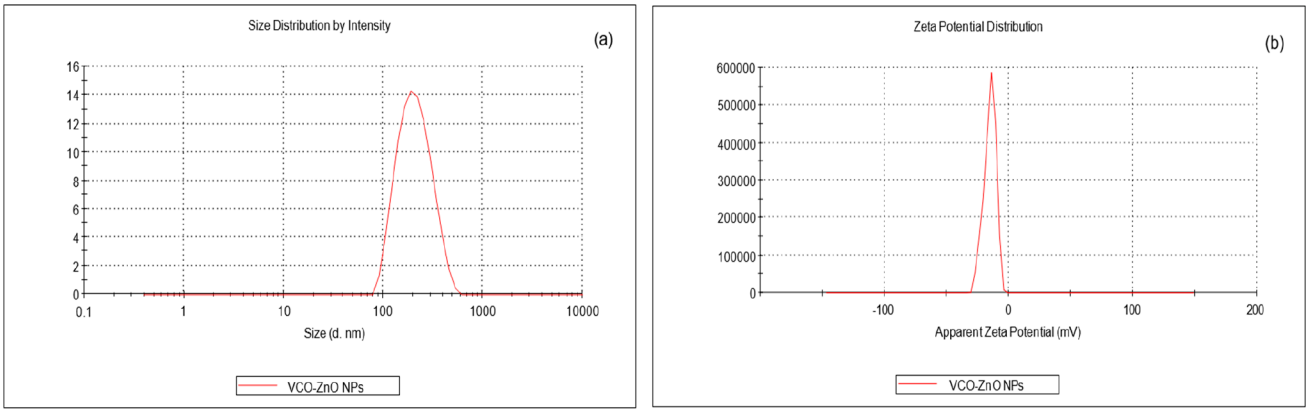

Figure 11. Dynamic light scattering (DLS) analysis of VCO-ZnO NPs: (a) size distribution by intensity and (b) zeta potential distribution.

Table 11

precursor weight (mg)	10000
precursor molecular weight	287.56
nanoparticle molar mass	81.38
nanoparticles weight after drying (mg)	2400
weight (%) of NPs from EDS	99.5
yield (%)	84.38

of unreacted metals, making it a promising prospect.[44] The FESEM image in Figure 12 depicts the clear and distinct images of the synthesized VCO-ZnONPs. They are almost spherical with few rodlike morphologies. The size of NPs was calculated using ImageJ software and showed them to be in the range 60−90 nm.

3.10. Comparative Study with Results from Previous Literature. In the Introduction, the benefits of utilizing VCO as a reducing agent for the synthesis of ZnO NPs are highlighted. Unlike many plant extracts, the commercial availability of VCO in its purest form enhances efficiency and purity and saves time and energy. Conducting a comparative analysis with various synthesis methods for ZnO NPs as in Table 12 can offer valuable insights into the advantages of employing VCO over other biological or green reducing agents. This analysis may encompass factors such as method of extract preparation and NP synthesis, morphological comparisons, and effectiveness in biomedical applications.

In order to represent all of the studies in one table, various symbols and abbreviations have been adopted as shown in the footnote to Table 12.

3.11. Conclusion. In conclusion, metal nanoparticles have gained prominence across industries for medical applications due to their size-dependent properties. Conventional methods often entail high costs and environmental risks; therefore, a promising alternative is a green synthesis method. Choosing vegetable oils in the purest form like virgin coconut oil (VCO) may help overcome the limitations of green synthesis such as difficulties in plant collection and extract preparation. By utilizing bioreduction by biomolecules from VCO, renowned for its health benefits, it serves as an effective reducer and stabilizer for nanoparticles. The functional groups within VCO contribute to the reduction process and hinder nanoparticle

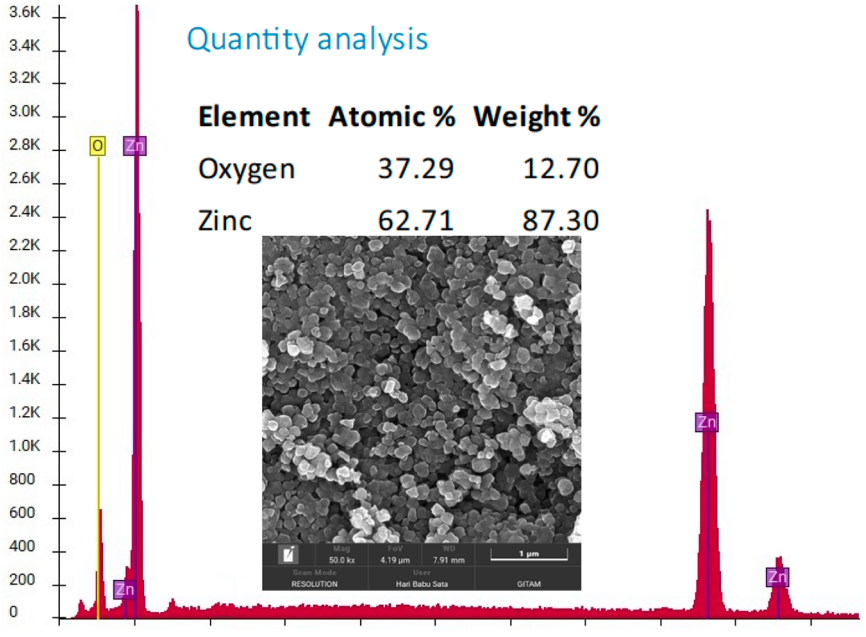

Figure 12. SEM and EDS analysis of VCO-ZnO NPs.

https://doi.org/10.1021/acsomega.4c01727
ACS Omega 2024, 9, 38396−38408

Table 12. Comparative Study of Benefits/Features of VCO over Other Reducing Agents in NP Synthesis with the Aid of Previous Literature[a]

reducing agent	extract method of reducing agent	synthesis method of NPs	particle size (nm)	application study	ref
VCO	cold pressed-commercially available	green gel combustion route	16	*IC_{50}, 78.9 μg/mL (DPPH); *POI, 38.9% at 40 μg/mL(DPPH); #IC_{50}, 22.4229 μg/mL (PDI); @IC_{50}, 88.45 μg/mL (α-amylase); ϕMIC, 0.156 mg/mL (PA), 0.316 mg/mL (SA); ϕZOI, 21.60 mm at 1 mg/mL (PA), 25.00 mm at 1 mg/mL (SA)	present work
almond oil	cold pressed-commercially available	chemical precipitation	35	*IC_{50}, 328.5 μg/mL (DPPH); ϕMIC, 0.3 mg/mL (PA)	45
Eucalyptus globulus Essential oil	hydrodistilled in a Clevenger apparatus	green precipitation using acetone dilution	24	ϕMIC, 2 mg/mL (PA)	46
clove buds	rotary evaporation method	green hydrothermal	50	*POI, 85% (DPPH); ϕZOI, 12 mm (SA)	47
Mentha pulegium essential oil	hydrodistillation using a Clevenger apparatus	chemical sol−gel method	nanofluid	ϕMIC, 3.3 ppm (SA)	48
M. fragrans fruit (nutmeg)			63	*POI, 66% at 0.4 mg/mL (DPPH); ϕZOI, 17 ± 1.66 mm (PA), 21 ± 1.73 mm (SA) at 1 mg/mL; @POI,73.23 ± 0.42 (α-amylase), 65.21 ± 0.49 (α-glucosidase) at 400 μg/mL	49
Medicago sativa L. (alfalfa)	boiling method	green combustion route method	10	*POI, 42.3% (DPPH); ϕMIC, 0.0093 mg/mL (*Candida*)	50
Aerva persica roots	rotary evaporation method	hydrothermal route	45	*POI, 91% at 0.25 mg/mL (DPPH); #POI, 79.76% at 36.5 mg/mL (carrageenan induced paw edema model)	51
aloe vera leaf	boiling and crude method	green precipitation	25−35		52
leaves of *H. fomes* (HF) and *S. apetala* (SA)	boiling method	green precipitation method	40−50	#IC_{50}, 63.29 μg/mL for SA-ZnO and 72.35 μg/mL for HF-ZnO (PDI); @IC_{50}, 334.4 μg/mL for SA-ZnO and 394.38 μg/mL for HF-ZnO (α-amylase)	53

[a]Abbreviations: POI, percentage of inhibition; PDI, protein denaturation inhibition; PA, *Pseudomonas aeruginosa* SA, *S. aureus*; ZOI, zone of inhibition. Symbols: *, characteristic values of antioxidant study; #, characteristic values of antiinflammatory study; @, characteristic values of antidiabetic study; ϕ, characteristic values of antimicrobial study.

https://doi.org/10.1021/acsomega.4c01727
ACS Omega 2024, 9, 38396−38408

agglomeration. Overall, the highlights of the work are the successful synthesis of ZnO NPs using VCO as a reducing as well as capping agent with zero chemical mediators and their biological properties which are comparable with those of standard medicines. These may make the synthesized ZnO NPs more suitable for use in the medical field. Further, the substantial nanoparticle yield indicates that the method has significant potential for large-scale production and commercialization. These key points open up possibilities for future research into producing other metal nanoparticles using VCO.

AUTHOR INFORMATION

Corresponding Author

K Ramachandra Rao − *Crystal Growth and Nano-Science Research Centre, Department of Physics, Government College (A), Rajamahendravaram, Andhra Pradesh 533105, India;* orcid.org/0000-0002-5400-4926; Email: ramc@gcrjy.ac.in, drkrcr@gmail.com

Authors

B. Durga Lakshmi − *Crystal Growth and Nano-Science Research Centre, Department of Physics, Government College (A), Rajamahendravaram, Andhra Pradesh 533105, India; Department of Physics, Adikavi Nannaya University, Rajamahendravaram, Andhra Pradesh 533296, India*

Betha Veera Vamsi Krishna − *Crystal Growth and Nano-Science Research Centre, Department of Physics, Government College (A), Rajamahendravaram, Andhra Pradesh 533105, India; Department of Physics, Adikavi Nannaya University, Rajamahendravaram, Andhra Pradesh 533296, India*

P. Tirupathi Rao − *Crystal Growth and Nano-Science Research Centre, Department of Physics, Government College (A), Rajamahendravaram, Andhra Pradesh 533105, India; Department of Physics, Adikavi Nannaya University, Rajamahendravaram, Andhra Pradesh 533296, India*

Abhinash Marukurti − *School of Life and Health Sciences, Adikavi Nannaya University, Rajamahendravaram, Andhra Pradesh 533296, India*

Vasudha K − *Crystal Growth and Nano-Science Research Centre, Department of Physics, Government College (A), Rajamahendravaram, Andhra Pradesh 533105, India*

Esub Basha Sk − *Crystal Growth and Nano-Science Research Centre, Department of Physics, Government College (A), Rajamahendravaram, Andhra Pradesh 533105, India*

Complete contact information is available at: https://pubs.acs.org/10.1021/acsomega.4c01727

Author Contributions

B.D.L.: Iinvestigation, resources, writing the manuscript. P.T.R.: visualization, writing the manuscript. B.V.V.K.: visualization, investigation. A.M.: investigation, data curation, writing the manuscript. E.B.S. and V.K.: visualization, investigation. K.R.R.: supervision, conceptualization, methodology, reviewing the manuscript.

Notes

The authors declare no competing financial interest.

ACKNOWLEDGMENTS

The authors are thankful to the Central Instrumentation Laboratory (CIL), Government College (A) Rajamahendravaram for providing the necessary facilities during the research work.

REFERENCES

(1) Ying, S.; Guan, Z.; Ofoegbu, P. C.; Clubb, P.; Rico, C.; He, F.; Hong, J. Green Synthesis of Nanoparticles: Current Developments and Limitations. *Environmental Technology & Innovation* **2022**, *26*, 102336.

(2) Nasrullah, M.; Gul, F. Z.; Hanif, S.; Mannan, A.; Naz, S.; Ali, J. S.; Zia, M. Green and Chemical Syntheses of CdO NPs: A Comparative Study for Yield Attributes, Biological Characteristics, and Toxicity Concerns. *ACS Omega* **2020**, *5* (11), 5739−5747.

(3) Ngampeerapong, C.; Chavasit, V.; Durst, R. W. Bioactive and Nutritional Compounds in Virgin Coconut Oils.*Malaysian J. Nutrition* **2018**, *24*, 257−267.

(4) Iranloye, B.; Oludare, G.; Olubiyi, M. Anti-Diabetic and Antioxidant Effects of Virgin Coconut Oil in Alloxan Induced Diabetic Male Sprague Dawley Rats. *JDM* **2013**, *03* (04), 221−226.

(5) Nitbani, F. O.; Tjitda, P. J. P.; Nitti, F.; Jumina, J.; Detha, A. I. R. Antimicrobial Properties of Lauric Acid and Monolaurin in Virgin Coconut Oil: A Review. *ChemBioEng. Reviews* **2022**, *9* (5), 442−461.

(6) Zamiri, R.; Zamiri, R.; Sadrolhosseini, A. R. Preparation of Silver Nanoparticles in Virgin Coconut Oil Using Laser Ablation. *IJN* **2011**, 71.

(7) Tang, K. S. The Current and Future Perspectives of Zinc Oxide Nanoparticles in the Treatment of Diabetes Mellitus. *Life Sciences* **2019**, *239*, 117011.

(8) Spoială, A.; Ilie, C.-I.; Truşcă, R.-D.; Oprea, O.-C.; Surdu, V.-A.; Vasile, B. Ş; Ficai, A.; Ficai, D.; Andronescu, E.; Diţu, L.-M. Zinc Oxide Nanoparticles for Water Purification. *Materials* **2021**, *14* (16), 4747.

(9) Sharma, D. K.; Shukla, S.; Sharma, K. K.; Kumar, V. A Review on ZnO: Fundamental Properties and Applications. *Materials Today: Proceedings* **2022**, *49*, 3028−3035.

(10) Walton, I. M.; Cox, J. M.; Benson, C. A.; Patel, D. D. G.; Chen, Y.-S.; Benedict, J. B. The Role of Atropisomers on the Photo-Reactivity and Fatigue of Diarylethene-Based Metal-Organic Frameworks. *New J. Chem.* **2016**, *40* (1), 101−106.

(11) Ansari, S. A.; Khan, M. M.; Ansari, M. O.; Lee, J.; Cho, M. H. Biogenic Synthesis, Photocatalytic, and Photoelectrochemical Performance of Ag-ZnO Nanocomposite. *J. Phys. Chem. C* **2013**, *117* (51), 27023−27030.

(12) Xie, J.; Li, H.; Zhang, T.; Song, B.; Wang, X.; Gu, Z. Recent Advances in ZnO Nanomaterial-Mediated Biological Applications and Action Mechanisms. *Nanomaterials* **2023**, *13* (9), 1500.

(13) Kshirsagar, A.; Khanna, T.; Dhanwe, V.; Kate, K. H.; Khanna, P. K. Green Synthesis of Silver Nano-Particles by Use of Edible Oils. *j nanosci nanotechnol* **2018**, *18* (1), 386−393.

(14) Meena Kumari, M.; Philip, D. Facile One-Pot Synthesis of Gold and Silver Nanocatalysts Using Edible Coconut Oil. *Spectrochimica Acta Part A: Molecular and Biomolecular Spectroscopy* **2013**, *111*, 154−160.

(15) Vinicius De Oliveira Brisola Maciel, M.; Da Rosa Almeida, A.; Machado, M. H.; Elias, W. C.; Gonçalves Da Rosa, C.; Teixeira, G. L.; Noronha, C. M.; Bertoldi, F. C.; Nunes, M. R.; Dutra De Armas, R.; Manique Barreto, P. L. Green Synthesis, Characteristics and Antimicrobial Activity of Silver Nanoparticles Mediated by Essential Oils as Reducing Agents. *Biocatalysis and Agricultural Biotechnology* **2020**, *28*, 101746.

(16) Khanna, P. K.; Nair, C. K. K. Synthesis of Silver Nanoparticles Using Cod Liver Oil (Fish Oil): Green Approach to Nanotechnology. *International Journal of Green Nanotechnology: Physics and Chemistry* **2009**, *1* (1), P3−P9.

(17) Kumar, B.; Smita, K.; Cumbal, L.; Debut, A. Sacha Inchi (Plukenetia Volubilis L.) Oil for One Pot Synthesis of Silver Nanocatalyst: An Ecofriendly Approach. *Industrial Crops and Products* **2014**, *58*, 238−243.

(18) Jiang, Z.; Li, L.; Huang, H.; He, W.; Ming, W. Progress in Laser Ablation and Biological Synthesis Processes: "Top-Down" and "Bottom-Up" Approaches for the Green Synthesis of Au/Ag Nanoparticles. *IJMS* **2022**, *23* (23), 14658.

(19) Ar, G. Antioxidant Activity of Some Medicinal Species Using FRAP Assay. *J. Medicinal Plants* **2011**, *10*, 54−60.
(20) Goodarzi, S.; Rafiei, S.; Javadi, M.; Haghighian, H. K.; Noroozi, S. A Review on Antioxidants and Their Health Effects. *J. Nutrition Food Security* **2018**, *3*, 106−112
(21) Vamsi Krishna, B. V.; Tirupathi Rao, P.; Durga Lakshmi, B.; Vasudha, K.; Esub Basha, Sk.; Putra Kumar, B.; Kiran, P. S. S.; Shreyas Chandra, K.; R K, R. Green Fabrication of Tinospora Cordifolia-Derived MgO Nanoparticles: Potential for Diabatic Control and Oxidant Protection. *Next Materials* **2024**, *3*, 100171.
(22) Ansari, S. A.; Khan, M. M.; Lee, J.; Cho, M. H. Highly Visible Light Active Ag@ZnO Nanocomposites Synthesized by Gel-Combustion Route. *Journal of Industrial and Engineering Chemistry* **2014**, *20* (4), 1602−1607.
(23) Khuda, F.; Jamil, M.; Ali Khan Khalil, A.; Ullah, R.; Ullah, N.; Naureen, F.; Abbas, M.; Shafiq Khan, M.; Ali, S.; Muhammad Umer Farooqi, H.; Ahn, M.-J. Assessment of Antioxidant and Cytotoxic Potential of Silver Nanoparticles Synthesized from Root Extract of Reynoutria Japonica Houtt. *Arabian Journal of Chemistry* **2022**, *15* (12), 104327.
(24) Syafitri, E.; Dalimunthe, A.; Silalahi, J. The Antioxidant Activity of Virgin Coconut Oil Using the FRAP, ABTS, CUPRAC, and DPPH Methods. *Pharma Innovation* **2023**, *12* (11), 21−25.
(25) Molyneux, P. The Use of the Stable Free Radical Diphenylpicryl- Hydrazyl (DPPH) for Estimating Antioxidant Activity. *Songklanakarin Journal of Science and Technology* **2004**, *26* (2) .1
(26) AAT Bioquest, Inc., IC50 Calculator, 2024. https://www.aatbio.com/tools/ic50-calculator.
(27) Gunathilake, K.; Ranaweera, K.; Rupasinghe, H. Influence of Boiling, Steaming and Frying of Selected Leafy Vegetables on the In Vitro Anti-Inflammation Associated Biological Activities. *Plants* **2018**, *7* (1), 22.
(28) K, V.; D, A.; B, M.; B, K. PHYTOCHEMICAL SCREENING, ANTIMICROBIAL, AND ANTIOXIDANT ACTIVITIES OF ROOT AND LEAF EXTRACTS OF LEUCAS ASPERA. *Asian J. Pharm. Clin Res.* **2019**, 141−147.
(29) Shalaby, E. A.; Shanab, S. M. M.; El-Raheem, W. M. A.; Hanafy, E. A. Biological Activities and Antioxidant Potential of Different Biosynthesized Nanoparticles of Moringa Oleifera. *Sci. Rep* **2022**, *12* (1), 18400.
(30) Vinotha, V.; Iswarya, A.; Thaya, R.; Govindarajan, M.; Alharbi, N. S.; Kadaikunnan, S.; Khaled, J. M.; Al-Anbr, M. N.; Vaseeharan, B. Synthesis of ZnO Nanoparticles Using Insulin-Rich Leaf Extract: Anti-Diabetic, Antibiofilm and Anti-Oxidant Properties. *Journal of Photochemistry and Photobiology B: Biology* **2019**, *197*, 111541.
(31) Balan, K.; Qing, W.; Wang, Y.; Liu, X.; Palvannan, T.; Wang, Y.; Ma, F.; Zhang, Y. Antidiabetic Activity of Green Synthesis Silver Nanoparticles Using Lonicera Japonica Leaves Extract. *RSC Adv.* **2016**, *6*, 40162.
(32) Singla, M. L.; Shafeeq M, M.; Kumar, M. Optical Characterization of ZnO Nanoparticles Capped with Various Surfactants. *J. Lumin.* **2009**, *129* (5), 434−438.
(33) Makuła, P.; Pacia, M.; Macyk, W. How To Correctly Determine the Band Gap Energy of Modified Semiconductor Photocatalysts Based on UV-Vis Spectra. *J. Phys. Chem. Lett.* **2018**, *9* (23), 6814−6817.
(34) Guo, L.; Yang, S.; Yang, C.; Yu, P.; Wang, J.; Ge, W.; Wong, G. K. L. Highly Monodisperse Polymer-Capped ZnO Nanoparticles: Preparation and Optical Properties. *Appl. Phys. Lett.* **2000**, *76* (20), 2901−2903.
(35) Alamdari, S.; Jafar Tafreshi, M.; Sasani Ghamsari, M.; Majles Ara, M. H. Preparation and Characterization of ZnO and CWO Nanopowders for Radiation Sensing. *Progress in Physics of Applied Materials* **2021**, *1*, 14−18.
(36) Dayrit, F. M. Lauric Acid Is a Medium-Chain Fatty Acid, Coconut Oil Is a Medium-Chain Triglyceride. *Phillippine J. Sci.***2014**, *143* (2), 157−166
(37) Apak, R.; Güçlü, K.; Demirata, B.; Özyürek, M.; Çelik, S.; Bektaşoğlu, B.; Berker, K.; Özyurt, D. Comparative Evaluation of Various Total Antioxidant Capacity Assays Applied to Phenolic Compounds with the CUPRAC Assay. *Molecules* **2007**, *12* (7), 1496−1547.
(38) Shah, P.; Modi, H. A. Comparative Study of DPPH, ABTS and FRAP Assays for Determination of Antioxidant Activity. *Chemistry, Environmental Science, Medicine* **2015**, *3*, 1
(39) Dorsey, B. M. Healthy Components of Coffee Processing by-Products In *Handbook of Coffee Processing By-Products* Elsevier: 2017; Chapter 2, p 27.
(40) Rumpf, J.; Burger, R.; Schulze, M. Statistical Evaluation of DPPH, ABTS, FRAP, and Folin-Ciocalteu Assays to Assess the Antioxidant Capacity of Lignins. *Int. J. Biol. Macromol.* **2023**, *233*, 123470.
(41) Naseer, M.; Aslam, U.; Khalid, B.; Chen, B. Green Route to Synthesize Zinc Oxide Nanoparticles Using Leaf Extracts of Cassia Fistula and Melia Azadarach and Their Antibacterial Potential. *Sci. Rep* **2020**, *10* (1), 9055.
(42) Kumar, R.; Umar, A.; Kumar, G.; Nalwa, H. S. Antimicrobial Properties of ZnO Nanomaterials: A Review. *Ceram. Int.* **2017**, *43* (5), 3940−3961.
(43) Meißner, T.; Oelschlägel, K.; Potthoff, A. Implications of the Stability Behavior of Zinc Oxide Nanoparticles for Toxicological Studies. *Int. Nano Lett.* **2014**, *4* (3), 116.
(44) Nasrullah, M.; Gul, F. Z.; Hanif, S.; Mannan, A.; Naz, S.; Ali, J. S.; Zia, M. Green and Chemical Syntheses of CdO NPs: A Comparative Study for Yield Attributes, Biological Characteristics, and Toxicity Concerns. *ACS Omega* **2020**, *5* (11), 5739−5747.
(45) Ramzan, I.; Bashir, M.; Saeed, A.; Khan, B. S.; Shaik, M. R.; Khan, M.; Shaik, B.; Khan, M. Evaluation of Photocatalytic, Antioxidant, and Antibacterial Efficacy of Almond Oil Capped Zinc Oxide Nanoparticles. *Materials* **2023**, *16* (14), 5011.
(46) Obeizi, Z.; Benbouzid, H.; Ouchenane, S.; Yılmaz, D.; Culha, M.; Bououdina, M. Biosynthesis of Zinc Oxide Nanoparticles from Essential Oil of Eucalyptus Globulus with Antimicrobial and Anti-Biofilm Activities. *Materials Today Communications* **2020**, *25*, 101553.
(47) Anvarinezhad, M.; Javadi, A.; Jafarizadeh-Malmiri, H. Green Approach in Fabrication of Photocatalytic, Antimicrobial, and Antioxidant Zinc Oxide Nanoparticles - Hydrothermal Synthesis Using Clove Hydroalcoholic Extract and Optimization of the Process. *Green Processing and Synthesis* **2020**, *9* (1), 375−385.
(48) Jahanpanahi, M.; Sani, A.M.; Sani, A. M.; Jahanpanahi, M. Antimicrobial Effect of Nanofluid Including Zinc Oxide (ZnO) Nanoparticles and Mentha Pulegium Essential Oil. *J. App Biol. Biotech* **2016**, 1.
(49) Faisal, S.; Jan, H.; Shah, S. A.; Shah, S.; Khan, A.; Akbar, M. T.; Rizwan, M.; Jan, F.; Wajidullah; Akhtar, N.; Khattak, A.; Syed, S. Green Synthesis of Zinc Oxide (ZnO) Nanoparticles Using Aqueous Fruit Extracts of *Myristica Fragrans*: Their Characterizations and Biological and Environmental Applications. *ACS Omega* **2021**, *6* (14), 9709−9722.
(50) Król, A.; Railean-Plugaru, V.; Pomastowski, P.; Buszewski, B. Phytochemical Investigation of Medicago Sativa L. Extract and Its Potential as a Safe Source for the Synthesis of ZnO Nanoparticles: The Proposed Mechanism of Formation and Antimicrobial Activity. *Phytochemistry Letters* **2019**, *31*, 170−180.
(51) Fatima, K.; Asif, M.; Farooq, U.; Gilani, S. J.; Bin Jumah, M. N.; Ahmed, M. M. Antioxidant and Anti-Inflammatory Applications of *Aerva Persica* Aqueous-Root Extract-Mediated Synthesis of ZnO Nanoparticles. *ACS Omega* **2024**, *9* (14), 15882−15892.
(52) Sangeetha, G.; Rajeshwari, S.; Venckatesh, R. Green Synthesis of Zinc Oxide Nanoparticles by Aloe Barbadensis Miller Leaf Extract: Structure and Optical Properties. *Mater. Res. Bull.* **2011**, *46* (12), 2560−2566.
(53) Thatoi, P.; Kerry, R. G.; Gouda, S.; Das, G.; Pramanik, K.; Thatoi, H.; Patra, J. K. Photo-Mediated Green Synthesis of Silver and Zinc Oxide Nanoparticles Using Aqueous Extracts of Two Mangrove Plant Species, Heritiera Fomes and Sonneratia Apetala and

https://doi.org/10.1021/acsomega.4c01727
ACS Omega 2024, 9, 38396−38408

Investigation of Their Biomedical Applications. *Journal of Photochemistry and Photobiology B: Biology* **2016**, *163*, 311−318.

https://doi.org/10.1021/acsomega.4c01727
ACS Omega 2024, 9, 38396−38408